JACS
JOURNAL OF THE AMERICAN CHEMICAL SOCIETY
Article
Cite This: J. Am. Chem. Soc. 2019, 141, 17637−17645
pubs.acs.org/JACS

Solution Phase and Surface Photoisomerization of a Hydrazone Switch with a Long Thermal Half-Life

Li-Qing Zheng,[†] Sirun Yang,[‡] Jinggang Lan,[§] Luzia Gyr,[†] Guillaume Goubert,[†] Hai Qian,[‡,∥] Ivan Aprahamian,*[,‡] and Renato Zenobi*[,†]

[†]Department of Chemistry and Applied Biosciences, ETH Zurich, Vladimir-Prelog-Weg 3, Zurich CH 8093, Switzerland
[‡]Department of Chemistry, Dartmouth College, Hanover, New Hampshire 03755, United States
[§]Department of Chemistry, University of Zurich, Winterthurerstrasse 190, Zurich CH 8057, Switzerland
[∥]Department of Chemistry, University of Illinois at Urbana−Champaign, 505 S Mathews Avenue, Urbana, Illinois, 61801, United States

Supporting Information

ABSTRACT: Photoswitches can be employed for various purposes, with the half-life being a crucial parameter to optimize for the desired application. The switching of a photochromic hydrazone functionalized with a C6 alkyl thiolate spacer (C6 HAT) was characterized on a number of metal surfaces. C6 HAT exhibits a half-life of 789 years in solution. Tip-enhanced Raman spectroscopy (TERS) was used to study the photoisomerization of the C6 HAT self-assembled monolayers (SAMs) on Au, Ag, and Cu surfaces. The unique spectroscopic signature of the *E* isomer at 1580 and 1730 cm^{-1} in TER spectra allowed for its discrimination from the *Z* isomer. It was found that C6 HAT switches on Au and Cu surfaces when irradiated with 415 nm; however, it cannot isomerize on Ag surfaces, unless higher energy light is used. Based on this finding, and supported by density functional theory calculations, we propose a substrate-mediated photoisomerization mechanism to explain the behavior of C6 HAT on these different metal surfaces. This insight into the hydrazone's switching mechanism on metal surfaces will contribute to the further exploitation of this new family photochromic compounds on metal surfaces. Finally, although we found that the thermal isomerization rate of C6 HAT drastically increases on metal surfaces, the thermal half-life is still 6.9 days on gold, which is longer than that of the majority of azobenzene-based systems.

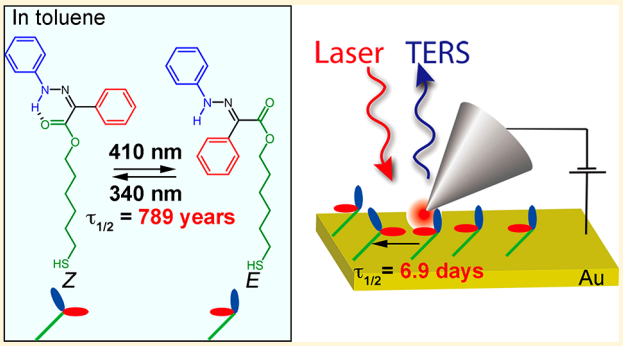

INTRODUCTION

Molecular switches play an important role in various fields, including biology, chemistry, materials science, and electronics,[1] because their structures and functions can be precisely controlled at the molecular level, using external stimuli, such as light, pH, or electric current.[2] These capabilities have made them very promising candidates for molecular electronics and high-density data storage applications.[3] Moreover, surfaces modified with molecular switches have been patterned and functionalized to act as regulators in organic field-effect transistors and organic light emitting diodes.[4] Various types of photoswitches have been investigated over the years for such and other applications, including azobenzenes,[7] diarylethenes,[8] spiropyrans,[9] and more recently hydrazones.[10] The thermal isomerization half-life of these systems is a crucial characteristic that determines the type of application for which they can be used.[5,6] While these switches have a wide range of thermal half-lives, ranging from microseconds to thousands of years in solution,[11,12] these values do not translate well when they are attached to metal surfaces, and in general a dramatic enhancement in isomerization rates is observed.[12a] For example, the thermal half-life of azobenzene derivatives decreases from 18.7 h in solution to 45.3 s when self-assembled on gold surfaces.[13] Consequently, photoswitches with very long thermal half-lives (e.g., bistable) are needed to build future devices. Investigating their molecular switching behavior on metal surfaces at the nanoscale can provide crucial information for future implementations.

When exposed to an external stimulus, molecular switches typically isomerize, for example, by undergoing a ring-closing/opening reaction,[14] or a *cis*/*trans* isomerization.[10,15] A great deal of work has been devoted to understanding the switching mechanism of molecules in solution[16,17] and the influence of solvent, temperature, and substituents on the outcome.[17a] However, when a molecular switch is attached to a metal surface, the new molecular environment and surface effects further complicate the switching mechanism.[18] For example,

Received: July 3, 2019
Published: October 12, 2019

DOI: 10.1021/jacs.9b07057
J. Am. Chem. Soc. 2019, 141, 17637−17645

switching in the solid state is inhibited to a certain degree as a result of steric hindrance. The metal surface can alter the switching mechanism of the adsorbed species. One reason for this is that excited adsorbates can relax via nonradiative decay, namely, via electron transfer to the conduction band of the surface and energy transfer to the Fermi level of the surface,[18b,19] leading to a decrease in the switching efficiency. For example, the observation that azobenzene fails to isomerize on Au (100) shows a strong surface effect.[20] Since molecular adsorbates can couple with the high density of states in the metal conduction band, the question arises whether there are other effects that interfere with the switching of molecules on metal surfaces upon light irradiation. For instance, Van Duyne and co-workers recently employed pump−probe surface-enhanced Raman spectroscopy (SERS) to demonstrate that photoinduced plasmons at a gold nanoparticle surface can drive the *trans*-to-*cis* isomerization of *trans*-1,2-bis(4-pyridyl) ethylene (BPE).[21]

To reveal the isomerization mechanism of molecular switches on a metal surface down to the single molecular layer level, analytical tools with high surface sensitivity and a low detection limit are needed. Tip-enhanced Raman spectroscopy (TERS) combines plasmon-enhanced Raman spectroscopy with scanning probe microscopy, and therefore provides chemical fingerprint information with high sensitivity and morphological information on the sample with nanometer spatial resolution.[22] TERS has recently been used to probe the isomerization of adsorbed azobenzene thiol (ABT), which was triggered by the bias voltage of a scanning tunneling microscope (STM) in ultrahigh vacuum.[23] Using ambient TERS, we reported that the photoisomerization yield of ABT molecules at Au grain boundaries is higher than that on Au terraces, due to reduced *cis*-to-*trans* back-reaction rate at the grain boundaries. The reduced back-reaction rate is a result of the lower reaction enthalpy of *trans*-to-*cis* isomerization at Au steps.[24] However, the lifetime of *cis* ABT on Au surfaces was found to be only 5 h, which is comparable to TERS acquisition times making the measurements difficult.

To address this issue, we decided to investigate the isomerization mechanism of recently developed bistable hydrazone photoswitches that exhibit thermal half-lives of up to 5000 years in solution.[5,12c] Herein, we first describe the molecular design of a hydrazone thiol (HAT) switch having a 6-carbon spacer (C6 HAT), allowing it to be conjugated to Au via thiol chemistry. Subsequently, we elaborate on the photoisomerization of HAT switches in solution, in the solid-state, and when assembled as a monolayer on a metal surface, using ultraviolet visible (UV−vis) spectroscopy and TERS. We used characteristic peaks in the Raman spectrum of C6 HAT to demonstrate its photoisomerization and quantitatively measured the extent of its switching using UV−vis spectroscopy. Furthermore, to reveal the photoisomerization mechanism of C6 HAT in a monolayer, we studied the isomerization of HAT on different metals (i.e., Au, Ag, and Cu). These studies, in corroboration with density functional theory (DFT) calculations, allowed us to propose a substrate-mediated isomerization mechanism to explain the different isomerization rates of C6 HAT on various metal surfaces.

RESULTS AND DISCUSSION

Molecular Design, Synthesis, and Solution Behavior. We chose a hydrazone skeleton[5] that has a half-life of 255 years in toluene in our design of C6 HAT. To minimize any electronic and steric effects on the hydrazone, the alkanethiol group was attached to the ester moiety of the switch. A 6 carbon chain linker (C6 HAT, Figure 1A) was selected to minimize the length of the molecule but still allow it to form a well-organized SAM on the surface.[25] C6 HAT was synthesized using a Mitsunobu reaction between an appropriate hydrazone derivative (Scheme S1) and 6-bromohexan-1-ol, followed by reaction with potassium thioacetate and deprotection with hydrazine in MeCN (56% yield). C6 HAT was fully characterized using NMR spectroscopy and high-resolution mass spectrometry (Figures S2−S5 in the Supporting Information).

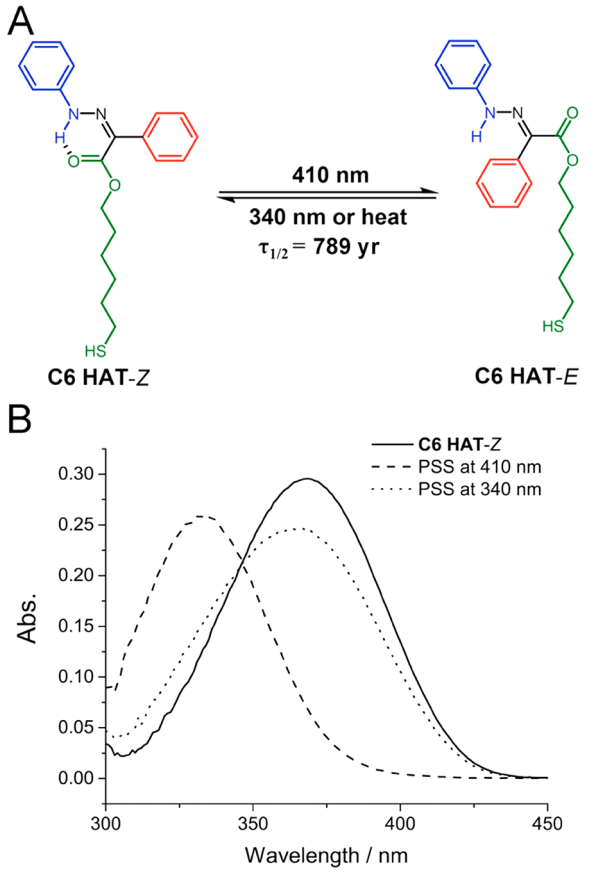

Figure 1. (A) Light induced *Z*/*E* isomerization of C6 HAT. (B) UV−vis spectra of C6 HAT in toluene (1×10^{-5} M) before (solid line) and after irradiation with 410 nm light (dashed line), followed by irradiation with 340 nm light (dotted line).

UV−vis spectroscopy was utilized to study the switching behavior of C6 HAT in toluene. The absorption spectrum of C6 HAT-*Z* shows a maximum (λ_{max}) at 368 nm (Figure 1b). Irradiation of the solution with 410 nm results in a shift of the λ_{max} to 333 nm. The photoisomerization efficiency of C6 HAT was studied using ^{1}H NMR spectroscopy. Upon 410 nm light irradiation, a sample of C6 HAT-*Z* yields a photostationary state (PSS) consisting of 98% C6 HAT-*E* isomer (Figure S6 in the Supporting Information). In addition to NMR spectroscopy, the ratio of *E* and *Z* isomers was calculated by fitting two Gaussian peaks to the UV−vis absorption spectrum. PSS_{410} of 96.5% C6 HAT-*E* were obtained by this fit, which is in good agreement with the NMR results (Figure S7 in the Supporting Information). The quantum yield (Φ) of the process was

DOI: 10.1021/jacs.9b07057
J. Am. Chem. Soc. 2019, 141, 17637−17645

determined to be 4.8 ± 0.1% (Figure S8 in the Supporting Information). The reverse switching can be induced by irradiation of the *E* rich sample with 340 nm light. The absorption maximum (λ_{max}) red-shifts to 364 nm with a PSS_{340} consisting of 74% (NMR spectroscopy) C6 HAT-*Z* isomer and a $\Phi_{E\rightarrow Z}$ of 9.4 ± 0.4% (Figure S9 in the Supporting Information). Fitting the absorption spectrum (dotted line in Figure 1B) yields a PSS_{340} containing 84% of the *Z* isomer (Figure S10 in the Supporting Information). The switching process was repeated 10 times by alternation of the irradiation wavelength between 410 and 340 nm. No signs of sample degradation were observed (Figure S11 in the Supporting Information). The half-life ($\tau_{1/2}$) of the *E* isomer was measured to be 789 ± 52 years at 298 K using a model compound (Table S1 in the Supporting Information).

Raman Spectroscopic Markers and Solid-State Photoisomerization. DFT calculations (B3LYP/6-31G*) were performed to predict the differences in the Raman spectra of the *Z* and *E* isomers of C6 HAT (Figure 2a).[26]

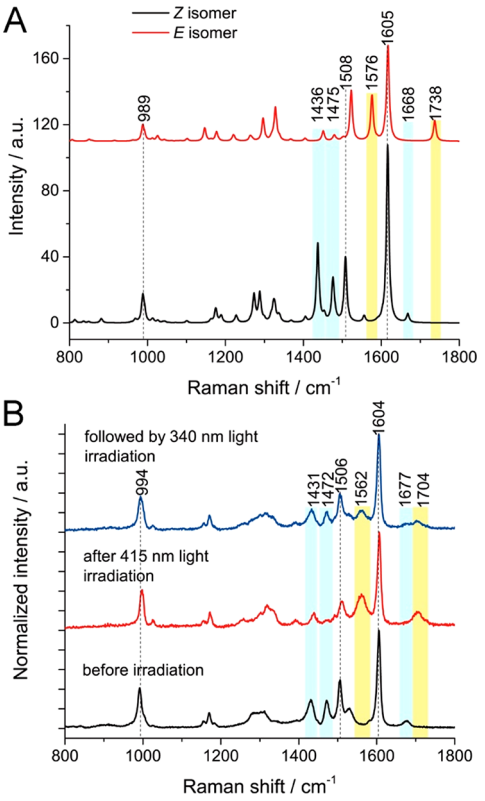

Figure 2. (A) Simulated Raman spectra of the *Z* and *E* isomers of C6 HAT. (B) Confocal Raman spectra of C6 HAT in the solid-state before and after irradiation at 415 nm, followed by irradiation at 340 nm. The light-blue bars indicate the Raman peaks at 1431, 1472, and 1677 cm^{-1}, which are characteristic for the *Z* isomer. The yellow bars indicate the Raman peaks at 1562 and 1704 cm^{-1} which are characteristic for the *E* isomer.

Theoretical frequencies were scaled by a factor of 0.98 to correct for anharmonicity.[27] The intensity of the Raman spectrum of the *E* isomer is half as strong as that of the *Z* one, most likely as a result of the loss of extended conjugation in the *E* isomer, which leads to a smaller Raman cross-section.[26] The Raman bands at 1436 and 1475 cm^{-1} ($\nu_{(C=N)}$) of the *Z* isomer shift to 1576 cm^{-1} upon isomerization. Moreover, the band at 1668 cm^{-1} ($\nu_{(C=O)}$) blue-shifts to 1738 cm^{-1} because of the disruption of the intramolecular H-bond (see Movies S1 and S2 in the Supporting Information). Upon *Z* → *E* isomerization, the C−N stretching mode slightly shifts from 1508 to 1522 cm^{-1} and a small peak appears at 1027 cm^{-1}. The bands at 1600 and 989 cm^{-1} correspond to the C=C stretching mode and the ring breathing mode of the benzene, respectively. Upon isomerization, these two peaks do not shift. Therefore, these two peaks were chosen as references.

Confocal Raman measurements on solid C6 HAT (powder of pure material, Figure 2B) are in good agreement with the calculated spectra. After 415 nm light irradiation, the intensity of the peak at 1431 cm^{-1} decreases, while the signals at 1472 and 1677 cm^{-1} disappear. Moreover, two new peaks appear at 1562 and 1704 cm^{-1}, and a smaller one appears at 1027 cm^{-1}. All these spectral changes indicate that the *Z* isomer underwent *Z* → *E* isomerization. The peaks at 994 and 1605 cm^{-1} remain the same.

Only the peak shift at 1522 cm^{-1}, predicted by DFT, is not observed. Overall, the Raman spectrum of C6 HAT, after irradiation at 415 nm, is in very good agreement with the calculated spectrum of the *E* isomer. Based on the intensity decrease in the bands at 1431, 1472, and 1677 cm^{-1}, almost 100% conversion from *Z* to *E* is achieved in the solid-state after 415 nm light irradiation. Upon further irradiation with 340 nm light, the intensities of the bands at 1431, 1472, and 1677 cm^{-1} partially recover. Meanwhile, the intensities of the peaks at 1562 and 1704 cm^{-1} decrease. Based on the peak area ratio between 1677 and 1704 cm^{-1} in the Raman spectrum, we can calculate the *Z* to *E* ratio to be 34:66 (see Figure S12), which is smaller than that observed in solution. Previously, we reported on the photoisomerization of another hydrazone switch in solution and in the solid state, monitored by UV−vis spectroscopy.[28] The switching efficiencies of C6 HAT obtained by UV−vis spectroscopy and Raman spectroscopy are comparable to our earlier results.[28]

Photoisomerization of a C6 HAT Monolayer on Au Surface. TER spectra of a C6 HAT SAM on a template stripped (TS) Au substrate before and after 415 nm light irradiation were collected, as shown in Figure 3A (top panel). After 415 nm light irradiation, the intensities of the peaks at 1430, 1472, and 1508 cm^{-1} decrease, while the intensities of the peaks at 1013 and 1050 cm^{-1} increase, and new peaks appear at 1580 and 1730 cm^{-1}. All these spectral changes indicate that *Z* → *E* isomerization occurred. To switch molecules back to the *Z* state, we heated the sample to 50 °C for 16 h and collected a TER spectrum afterward. The bands at 1430 and 1472 cm^{-1} recover, while the peak at 1580 cm^{-1} still remains, indicating that part of C6 HAT-*E* molecules isomerized back to the *Z* form (see Figure S13). In the TER spectra, no Raman peaks related to carbonaceous contaminants are observed, which indicates that neither UV irradiation nor laser irradiation induces any photodamage in C6 HAT. The assumption that there is no desorption of C6 HAT from the Au substrate upon UV irradiation was tested and confirmed by temperature-programmed desorption mass spectrometry (see Figures S14−S16).

We further collected TERS maps of C6 HAT SAMs on Au before and after 415 nm light irradiation (1 × 1 μm^2 size with a 32 × 32 nm^2 pixel size) to estimate the isomerization ratio. All 1064 TERS spectra within a map are displayed as a waterfall plot (Figure 3B) to highlight the spectral differences. In the TERS image of a C6 HAT SAM on Au prior to 415 nm light irradiation, the characteristic Raman peaks at 1430, 1472, and

DOI: 10.1021/jacs.9b07057
J. Am. Chem. Soc. 2019, 141, 17637−17645

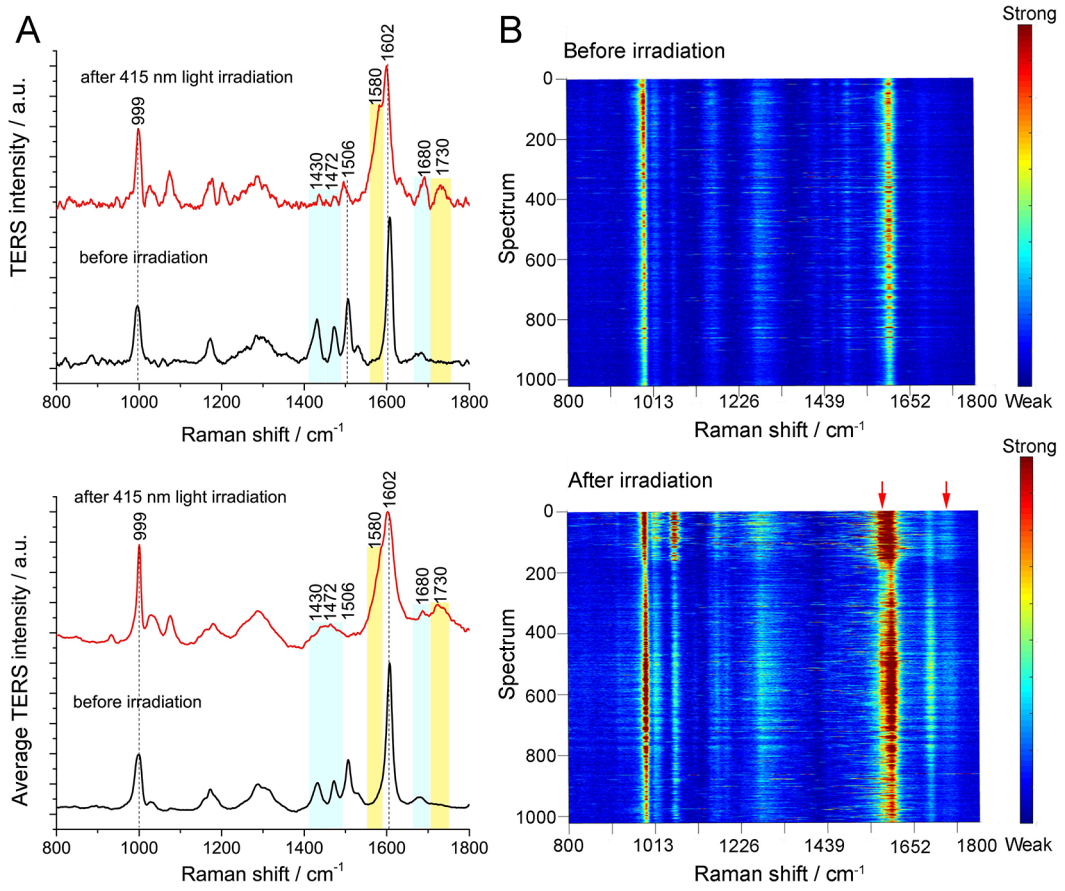

Figure 3. (A) Baseline corrected TER spectra (top panel) of a C6 HAT monolayer on a Au surface before (black) and after (red) 415 nm light irradiation, and average TER spectra (bottom panel) from the TERS maps of a C6 HAT monolayer on Au before (black) and after (red) 415 nm light irradiation. (B) Waterfall plot of all TER spectra from maps of a C6 HAT monolayer on Au before (top panel) and after (bottom panel) 415 nm light irradiation. The size of all maps is 1 × 1 μm^2 with a 31 nm pixel size. All TER spectra were normalized using the Raman peak at 1602 cm^{-1}.

Table 1. Photochemical Properties of C6 HAT

			monolayer on	
parameter	toluene	solid-state[a]	Au	Cu
λ_{max}, *Z*-isomer (nm)	368	–[b]	378	364
λ_{max}, *E*-isomer (nm)	333	–[b]	343	330
$([E]:[Z])_{PSS415}$ (%)	98:2	99:1	82:18	62:38
$([E]:[Z])_{PSS340}$ (%)	26:74	66:34	–[b]	–[b]
$\tau_{1/2}$[c]	789 ± 52 years	–[b]	6.90 ± 0.03 days	–[b]

[a]Powder sample. [b]Not determined. [c]Half-life of the thermal *E*-to-*Z* transformation.

1506 cm^{-1} of *Z*-C6 HAT are observed. However, because of the limited enhancement of the Ag tip used, the Raman band at 1680 cm^{-1}, which corresponds to the C═O stretching mode of the *Z* isomer, was invisible in this map (top panel of Figure 3B). We, therefore, recorded another TERS map, in which the peak at 1680 cm^{-1} is clearly observed, using another Ag tip with higher enhancement (Figure S17 in the Supporting Information). After irradiation at 415 nm, Raman peaks at 999, 1013, 1050, 1600, and 1680 cm^{-1} were clearly observed in the image, as shown in Figure 3B (bottom panel). Moreover, we could clearly see that the peaks at 1430 and 1472 cm^{-1} disappear and new signals arise at 1580 and 1730 cm^{-1} simultaneously. As shown in the TERS image (Figure S18 in Supporting Information), the peak at 1730 cm^{-1} appears in 79% of the spectra, indicating that some of the *Z*-C6 HAT molecules have isomerized to the *E* state. The isomerization ratio of the C6 HAT SAM is smaller than that of C6 HAT bulk material (see Table 1), which could result from electron or energy transfer from the excited states of C6 HAT to the Au surface.

All TER spectra within a map were accumulated and averaged to obtain statistical information (bottom panel of Figure 3A). The average TER spectra of C6 HAT SAM before and after irradiation at 415 nm show similar spectral features compared to the TER spectra shown in Figure 3A (top panel). Gaussian functions were fitted to the peaks at 1680 and 1730 cm^{-1} corresponding to the *Z* and *E* isomers, respectively. The area ratio of these two peaks was used to determine that 82% of the molecules in the SAM are in the *E* form (Table 1; Figure S19 in the Supporting Information), which is consistent with

DOI: 10.1021/jacs.9b07057
J. Am. Chem. Soc. 2019, 141, 17637−17645

the calculation based on the probability of the presence of the peak at 1580 cm^{-1} in the TERS map (Figure S18 in the Supporting Information). We also performed TERS line scans along Au grain edges and terraces with a 10 nm pixel size to measure the isomerization ratio at different sites (Figure S20 in the Supporting Information). The presence of the peak at 1580 cm^{-1} both on terraces and at grain edges indicates that photoisomerization can happen at both sites. Because of their low Raman cross-section, the peaks at 1680 or 1730 cm^{-1} were not observed in line-scan TER spectra.

The photoisomerization of C6 HAT SAMs on Au was further investigated by UV−vis spectroscopy. As shown in Figure 4, the maximum absorption peak of *Z*-C6 HAT SAM

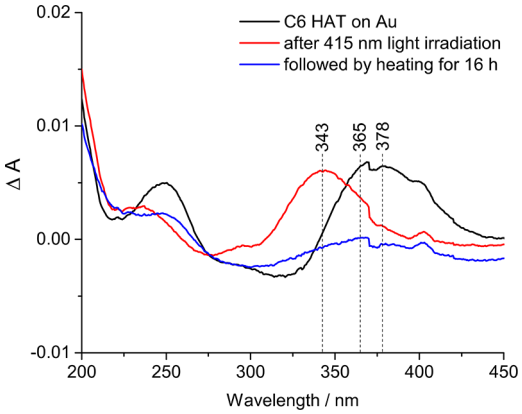

Figure 4. UV−vis spectra of a C6 HAT SAM on a Au surface before (black line) and after 415 nm light irradiation (red line). The blue line is the sample after heating under dark for 16 h.

appears at 378 nm. Upon 415 nm light irradiation, it shifts to 343 nm, which indicates that $Z \rightarrow E$ isomerization has taken place. The sample was then heated to 50 °C for 16 h, which resulted in a shift of the λ_{max} back to 365 nm and a decrease of absorbance. This result indicates that most of the *E*-C6 HAT has isomerized back to the *Z* state. The absorbance decrease could be due to the desorption of C6 HAT molecules from the surface upon heating. The discrete steps at 370 and 420 nm are due to the change of grating. A control experiment was conducted to check whether irradiation at 340 nm can induce the *E*-to-*Z* isomerization of C6 HAT on Au surface. A C6 HAT SAM on Au was first irradiated with 415 nm light and then followed by irradiation at 340 nm. The absorption peak of C6 HAT shifts back to 346 nm, which means that irradiation at 340 nm barely induce $E \rightarrow Z$ isomerization on the Au surface (see Figure S21).

The thermal lifetime of the *E* isomers on the Au surface is an important characteristic of the surface bound switch. The absorbance change at 340 nm of a C6 HAT SAM on a Au surface after 415 nm light irradiation as a function of time is shown in Figure S22. Analysis of the data shows that the thermal back isomerization on the surface is dominated by first-order kinetics with a rate constant of 1.16×10^{-6} s^{-1}. The half-life of the *E* isomer on the Au surface is thus around 6.90 ± 0.03 days, which is the longest value obtained for such systems, and higher than that of a recently reported azobenzene derivative on a Au surface.[13] As a thermodynamically unfavorable state, the long lifetime of the *E* form is attributed to the high energy barrier for the $E \rightarrow Z$ isomerization.[5] With such a relatively long thermal lifetime on the metal surface, it is a promising system toward the development of optical data storage devices.

Photoisomerization of a C6 HAT Monolayer on Ag or Cu Surface. To study the effect of the nature of the metal on the photoisomerization of a C6 HAT SAM, we also studied its isomerization on the Ag or Cu surface. A waterfall plot of the spectra extracted from TERS images of C6 HAT SAM on Ag before and after 415 nm light irradiation is shown in Figure S23. The average TER spectra are shown in Figure 5A, in which the Raman bands at 1430, 1473, 1506, and 1680 cm^{-1}, characteristic peaks for *Z*-C6 HAT, are still observed and no peaks appear at 1580 or 1730 cm^{-1}. This suggests that no $Z \rightarrow E$ isomerization of C6 HAT occurs on the Ag surface. Moreover, there is no absorption peak shift observed in the UV−vis spectrum of C6 HAT SAM on Ag after 415 nm light irradiation (Figure 5B), which is in agreement with the TERS results. Next we studied the isomerization of a C6 HAT SAM on a Cu surface. As shown in Figure 5C, after 415 nm light irradiation, we can clearly see that the intensities of the peaks at 1430, 1473, and 1680 cm^{-1} decrease, with small peaks appearing at 1580 and 1730 cm^{-1} in the average TER spectrum of C6 HAT on Cu. The spectral change is seen more clearly in the waterfall plot of the TERS spectra extracted from images (see Figure S24). Gaussian functions were again fitted to the peaks at 1680 and 1730 cm^{-1} corresponding to *Z* and *E* isomers, respectively. Based on the area ratio of these two peaks, 62% of C6 HAT molecules in the SAM have isomerized (Table 1; see Figure S25 in the Supporting Information). The lower isomerization efficiency is the main reason why the average spectral change of the TERS spectrum of C6 HAT on Cu is smaller than that on the Au surface (see Table 1). Moreover, the molecular orientation of C6 HAT on Cu is different from that of C6 HAT on Au. In Figure 5C, the new peaks that appear at 1576 and 1732 cm^{-1} are less obvious than the peak intensity decrease at 1427 and 1470 cm^{-1}, which is likely due to the surface selection rules of TERS. The UV−vis spectroscopic results also support this observation. As shown in Figure 5D, the blue-shift of the absorption maximum from 364 to 330 nm was seen after 415 nm light irradiation, which indicates that C6 HAT molecules on Cu surface underwent $Z \rightarrow E$ isomerization. The obtained sample was then heated to 50 °C for 16 h. The absorption maximum was found to shift to 339 nm, which indicates only a partially isomerization of *E*-C6 HAT to the *Z* form. The discrete step at 330 nm (blue spectrum) is due to the change from a tungsten lamp to a deuterium lamp during measurement. A control experiment was conducted to check whether irradiation at 340 nm can induce the *E*-to-*Z* isomerization of C6 HAT on a Cu surface. It is shown that irradiation by 340 nm light barely induce $E \rightarrow Z$ isomerization on the Cu surface, which is similar to the case of C6 HAT on Au (see Figure S26 in the Supporting Information).

Substrate-Mediated Photoisomerization Mechanism. The first possible isomerization mechanism that we evaluated (Figure 6A) is the direct photoexcitation of C6 HAT on the metal surfaces. Because of the quenching effects of metal surfaces, the isomerization of C6 HAT through direct molecular photoexcitation is suppressed, although to different degrees, by the metal surfaces. The failure of the isomerization of C6 HAT on Ag surface and the decrease in the isomerization efficiency of C6 HAT on the Au surface compared to the solid-state are indications of this phenomenon. A drop in isomerization efficiency could also result from

DOI: 10.1021/jacs.9b07057
J. Am. Chem. Soc. 2019, 141, 17637−17645

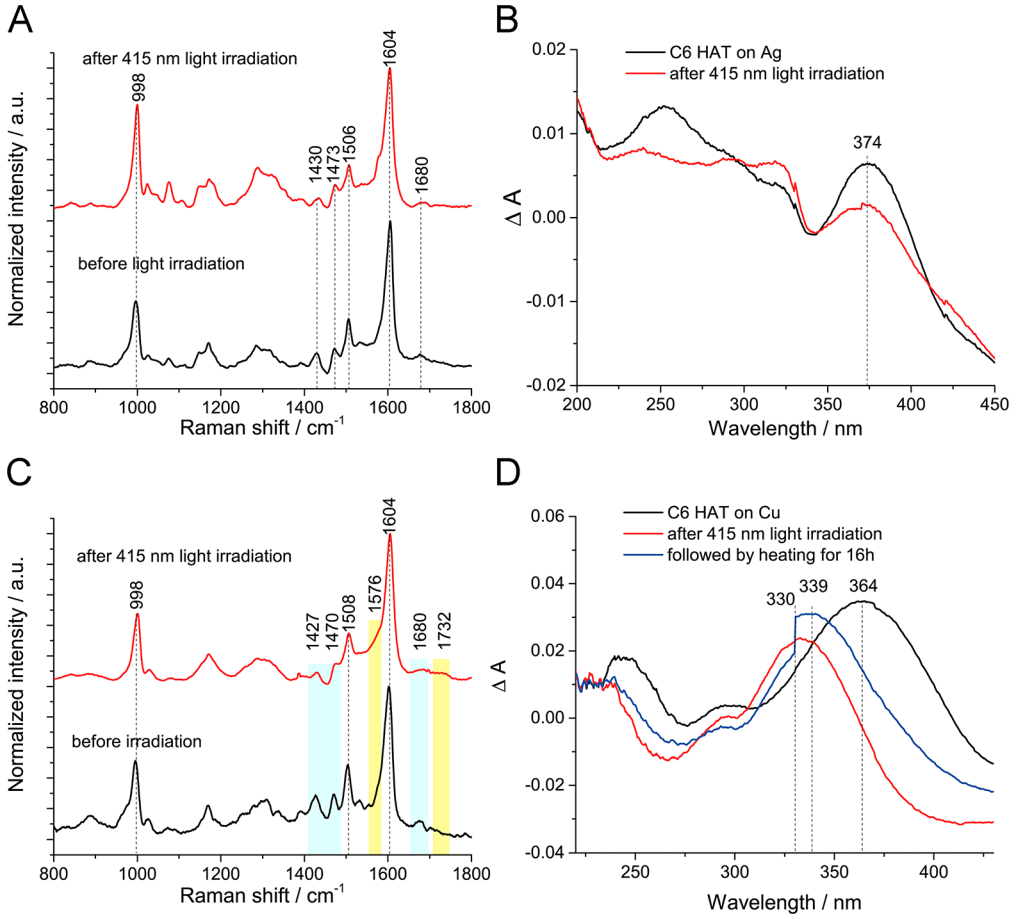

Figure 5. (A) Baseline corrected average TER spectra from the TERS maps of a C6 HAT SAM on a Ag surface before and after 415 nm light irradiation. (B) UV−vis spectra of a C6 HAT SAM on a Ag surface before (black line) and after 415 nm light irradiation (red and blue lines). (C) Baseline corrected average TER spectra from the TERS maps of a C6 HAT SAM on a Cu surface before and after 415 nm light irradiation. (D) UV−vis spectra of a C6 HAT SAM on a Cu surface before (black line) and after 415 nm light irradiation (red line). The sample was then kept in the dark and heated to 50 °C for 16 h (blue line). The size of all the maps is 1 × 1 μm^2.

steric hindrance. To exclude this effect, we investigated the isomerization of C6 HAT on Ag diluted in a 10-fold excess of hexanethiol using UV−vis spectroscopy. As shown in Figure S27, the maximum absorbance of C6 HAT did not shift upon 415 nm light irradiation, indicating that C6 HAT molecules with a lower packing density on Ag cannot isomerize to the *E* form. Therefore, failure of the photoisomerization of C6 HAT on Ag must stem from electronic rather than steric effects. The fact that C6 HAT SAM can isomerize on Au and Cu with 415 nm light irradiation also supports this interpretation. The second possible mechanism is a substrate-mediated photoisomerization mechanism[29] in which the electronic structure of the molecules, and the density of states (DOS) of the substrate should be taken into account. Tegeder and co-workers proposed such a mechanism for the photoisomerization of tetra-*tert*-butyl-azobenzene (TBA) physically absorbed on a Au surface.[29] UV light first generates hot holes in the Au d-band, which subsequently relax to the top of the d-band through Auger decay. These hot holes then undergo a charge transfer to the HOMO of TBA, leading to the formation of transient positive ions, which may subsequently result in the isomerization of TBA. Based on this theory, we calculated the orbital energy levels of C6 HAT bound to the different metal surfaces and the DOS of the different metals using density functional theory (DFT) (see Figures S28 and S29) As shown in Figure 6B, the top of the d-band of Au is at 2.2 eV, which overlaps with the second HOMO (HOMO-2) of C6 HAT. We speculate that 415 nm light (E = 3 eV) irradiation generates hot holes in the Au d-band, which first relax to the top of the d-band and can then transfer to C6 HAT to form transient positive ions, leading to the isomerization of C6 HAT. In the case of Ag, because of the lower lying d-band (d-band edge of Ag is 3.9 eV), light-induced switching cannot be achieved with 415 nm light irradiation (Figure 6C). In contrast, the d-band edge of Cu is at 2.1 eV, so 415 nm light irradiation can induce the isomerization of C6 HAT SAM on Cu. (Figure 6D) Regarding the hot carrier transfer process from substrate to the C═N switchable group of C6 HAT, our hypothesis is that it occurs via direct electron tunneling. Our system is a typical donor−bridge−acceptor system,[30] in which the alkyl chain serves as the bridge between the metal substrate and the switchable group of C6 HAT. It is well-known that in such a system, coherent electron tunneling from donor to acceptor can take place via virtual states in the bridge, referred to as superexchange mechanism.[30,31] Based on Marcus theory, the electron transfer rate decays exponentially with donor−acceptor distance.[30a,c,32] In our case, the distance between the donor and acceptor is only ca. 10 Å. For comparison, Murray et al. reported that the conductivity of Au clusters protected by an alkanethiol monolayer with a 6-carbon chain

DOI: 10.1021/jacs.9b07057
J. Am. Chem. Soc. 2019, 141, 17637−17645

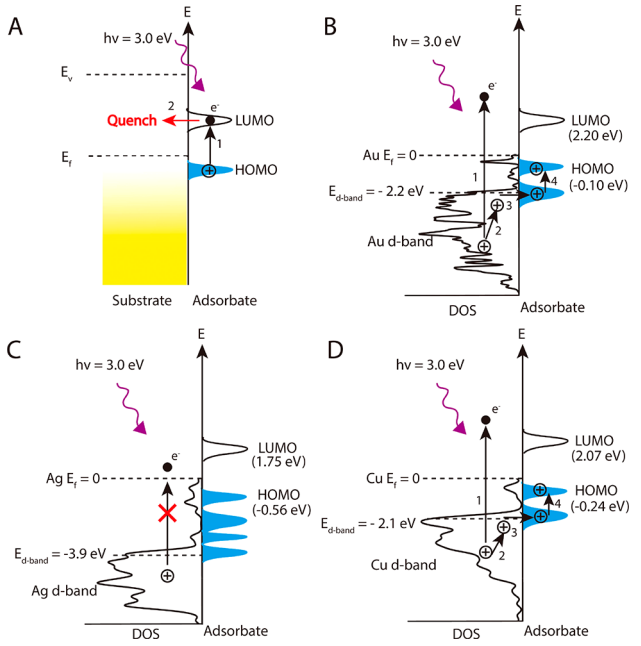

Figure 6. (A) Possible excitation and quenching mechanisms in the photoisomerization of a C6 HAT SAM at different metal surfaces. (B–D) Proposed excitation mechanism for the photoisomerization of a C6 HAT SAM at different metal surfaces.

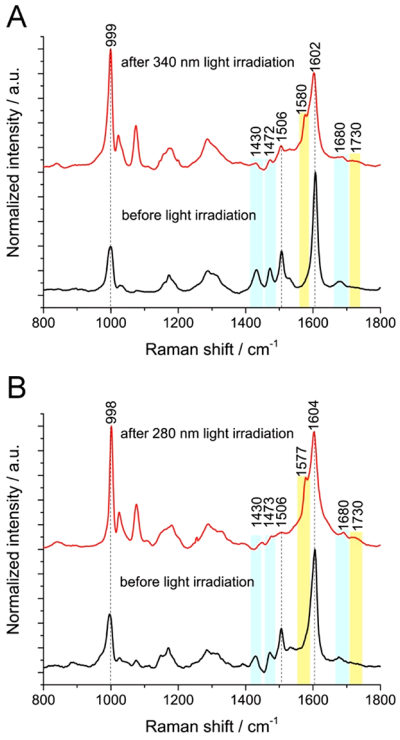

Figure 7. (A) Baseline corrected average TER spectra from the TERS maps of a C6 HAT SAM on a Au surface before and after 340 nm light irradiation. (B) Baseline corrected average TER spectra from the TERS maps of a C6 HAT SAM on a Ag surface before and after 280 nm light irradiation. The size of all maps is 1 × 1 μm^2 with a 31 nm pixel size.

was ca. 1.8×10^{-4} and 6.6×10^{-4} Ω^{-1} cm^{-1} depending on the size of the Au clusters.[30a] Therefore, direct electron tunneling from the Au surface to the C═N switchable group of C6 HAT is clearly feasible.

To further verify the substrate-mediated photoisomerization mechanism, we irradiated the C6 HAT SAM on Au with 340 nm light (E = 3.65 eV), and the C6 HAT SAM on Ag with 280 nm light (E = 4.4 eV), respectively, to induce the $Z \rightarrow E$ photoisomerization. As shown in Figure 7A, after 340 nm light irradiation, we can clearly see the intensity drop of the peaks at 1430, 1472, 1506, and 1680 cm^{-1}, and new peaks appearing at 1580 and 1730 cm^{-1} in the average TER spectrum of C6 HAT on Au. These spectral changes indicate that $Z \rightarrow E$ isomerization took place, which is in agreement with the substrate-mediated mechanism. In contrast, 340 nm light irradiation induces $E \rightarrow Z$ isomerization in solution, showing that there is a large difference in the solution phase and monolayer switching behavior. According to the substrate-mediated mechanism, light irradiation with energy above 3.9 eV should induce $Z \rightarrow E$ isomerization of C6 HAT on Ag surface. The average TER spectra of C6 HAT SAM on Ag before and after 280 nm light irradiation are shown in Figure 7B. The intensity of peaks at 1430, 1473, and 1506 cm^{-1} drops, and new peaks come out at 1577 and 1730 cm^{-1}, which is quite different from the TER spectrum when irradiating with 415 nm light (Figure 5A). This suggests that C6 HAT molecules isomerized to the E form with 280 nm light irradiation. In contrast, solid-phase C6 HAT cannot isomerize from the Z to the E form upon irradiation by either 340 or 280 nm light (Figure S30). Moreover, irradiating a C6 HAT solution with 280 nm light cannot induce $Z \rightarrow E$ isomerization (Figure S31). Only a very tiny and negligible proportion of Z-C6 HAT isomerizes to the E form in solution upon irradiation with 340 nm light because of the small absorption of Z-C6 HAT at this wavelength (see Figure S32). These results support our proposed substrate-mediated photoisomerization mechanism.

CONCLUSIONS

A new bistable ($\tau_{1/2}$ = 789 years) hydrazone photoswitch having a C6 alkyl thiolate linker (C6 HAT) was synthesized, and its switching behavior was studied in solution, in the solid-state and as a monolayer on various metal surfaces using confocal Raman, TERS, and UV–vis spectroscopies. Interestingly, C6 HAT can isomerize on Au and Cu surfaces, but not on Ag upon irradiation by 415 nm light (E = 3 eV). Higher energy light is required to activate the switch on Ag. Based on these findings, we propose a substrate-mediated charge transfer mechanism for the isomerization of C6 HAT on metal surfaces. This mechanism is supported by DFT calculations and TERS results. In this process, the length of the carbon linker plays an important role. When increasing the carbon chain length, the proposed substrate-mediated photoisomerization mechanism would stop working at a certain distance, since the electron transfer rate decays exponentially with donor–acceptor distance. However, photoswitches are still able to isomerize at larger distances via direct photoexcitation, because at larger distances there is less quenching by the surface. Thus, the length of the carbon is a critical parameter to maximize the isomerization efficiency on metal surfaces. As for the $E \rightarrow Z$ isomerization, it can be thermally activated, with a half-life of 6.9 days (at room temperature) on the Au surface. This is the longest thermal half-life ever measured for photoswitches on metal surfaces. The lifetime of the E molecules may depend on the nature of the metal, and on

DOI: 10.1021/jacs.9b07057
J. Am. Chem. Soc. 2019, 141, 17637–17645

the linker length.[13] The details of the relaxation mechanism are a topic that will require future studies to be clarified. This property, in addition to the ease of synthesis and assembly of the switches on metal surfaces, and very good separation of the Raman bands of the *Z* and *E* isomers, make this system highly valuable in the development of photocontrollable surfaces. One immediate application might be surface patterning using the photoswitches and using TERS for the in situ imaging of the UV light initiated surface isomerization.

■ ASSOCIATED CONTENT

Supporting Information

The Supporting Information is available free of charge on the ACS Publications website at DOI: 10.1021/jacs.9b07057.

Experimental details, chemical synthesis, photoisomerization studies in toluene solution, desorption analysis by MS, TERS study of the isomerization of a C6 HAT SAM, thin-film UV−vis spectroscopic study, theoretical calculations, and confocal Raman spectrum analysis (PDF)

Vibrational modes of the *E* isomers (MP4)

Vibrational modes of the *Z* isomers (MP4)

■ AUTHOR INFORMATION

Corresponding Authors

*ivan.aprahamian@dartmouth.edu

*renato.zenobi@org.chem.ethz.ch

ORCID

Guillaume Goubert: 0000-0002-4325-0267

Ivan Aprahamian: 0000-0003-2399-8208

Renato Zenobi: 0000-0001-5211-4358

Notes

The authors declare no competing financial interest.

The original data used in this publication are made available in a curated data archive at ETH Zurich (https://www.research-collection.ethz.ch) under the DOI: 10.3929/ethz-b-000353526.

■ ACKNOWLEDGMENTS

We thank Hao Yin (Xiamen University) and Jonas Bastian Metternich (ETH Zurich) for insightful discussions, Tian Liu (ETH Zurich), Dr. Alessandro Lauria (ETH Zurich), Madeleine Fellner (ETH Zurich) and Prof. Markus Niederberger (ETH Zurich) for UV−vis spectroscopy measurements, Jacek Szczerbiński (ETH Zurich) for TPD-MS measurements. L.-Q.Z. is indebted to the Chinese Scholarship Council for a Ph.D. student fellowship. We thank the High Performance Computing Team at ETH Zurich for help with DFT calculations and the ERC program (Grant # 741431−2DNanoSpec) for financial support. I.A. is thankful to the National Science Foundation (CHE-1807428) for the generous support.

■ REFERENCES

(1) (a) Szymanski, W.; Beierle, J. M. H.; Kistemaker, A. V.; Velema, W. A.; Feringa, B. L. Reversible Photocontrol of Biological Systems by the Incorporation of Molecular Photoswitches. *Chem. Rev.* **2013**, *113*, 6114−6178. (b) Russew, M.-M.; Hecht, S. Photoswitches: From Molecules to Materials. *Adv. Mater.* **2010**, *22*, 3348−3360.

(2) (a) Fihey, A.; Perrier, A.; Browne, W. R.; Jacquemin, D. Multiphotochromic molecular systems. *Chem. Soc. Rev.* **2015**, *44*, 3719−3759. (b) Landge, S. M.; Aprahamian, I. A pH Activated Configurational Rotary Switch: Controlling the *E*/*Z* Isomerization in Hydrazones. *J. Am. Chem. Soc.* **2009**, *131*, 18269−18271. (c) Choi, B. Y.; Kahng, S. J.; Kim, S.; Kim, H.; Kim, H. W.; Song, Y. J.; Ihm, J.; Kuk, Y. Conformational Molecular Switch of the Azobenzene Molecule: A Scanning Tunneling Microscopy Study. *Phys. Rev. Lett.* **2006**, *96*, 156106.

(3) (a) Robertus, J.; Browne, W. R.; Feringa, B. L. Dynamic control over cell adhesive properties using molecular-based surface engineering strategies. *Chem. Soc. Rev.* **2010**, *39*, 354−378. (b) Zheng, Y. B.; Kiraly, B.; Cheunkar, S.; Huang, T. J.; Weiss, P. S. Incident-angle-modulated molecular plasmonic switches: a case of weak exciton−plasmon coupling. *Nano Lett.* **2011**, *11*, 2061−2065. (c) Balzani, V.; Credi, A.; Raymo, F. M.; Stoddart, J. F. Artificial molecular machines. *Angew. Chem., Int. Ed.* **2000**, *39*, 3348−3391.

(4) (a) Orgiu, E.; Samori, P. 25th anniversary article: organic electronics marries photochromism: generation of multifunctional interfaces, materials, and devices. *Adv. Mater.* **2014**, *26*, 1827−1845. (b) Jerca, V. V.; Hoogenboom, R. Photocontrol in Complex Polymeric Materials: Fact or Illusion? *Angew. Chem., Int. Ed.* **2018**, *57*, 7945−7947; . Jerca, V. V.; Hoogenboom, R. Steuerung komplexer Polymermaterialien mit Licht: Wirklichkeit oder Illusion? *Angew. Chem.* **2018**, *130*, 8073−8075; . (c) Ratner, M. Molecular electronics: Pushing electrons around. *Nature* **2000**, *404*, 137−138. (d) Cuniberti, G.; Fagas, F.; Richter, K. *Introducing Molecular Electronics*; Springer, Berlin, Heidelberg, 2005. (e) Gahl, C.; Brete, D.; Leyssner, F.; Koch, M.; McNellis, E. R.; Mielke, J.; Carley, R.; Grill, L.; Reuter, K.; Tegeder, P.; Weinelt, M. Coverage-and temperature-controlled isomerization of an imine derivative on Au (111). *J. Am. Chem. Soc.* **2013**, *135*, 4273−4281.

(5) Qian, H.; Pramanik, S.; Aprahamian, I. Photochromic hydrazone switches with extremely long thermal half-lives. *J. Am. Chem. Soc.* **2017**, *139*, 9140−9143.

(6) Hirshberg, Y. Reversible formation and eradication of colors by irradiation at low temperatures. A photochemical memory model. *J. Am. Chem. Soc.* **1956**, *78*, 2304−2312.

(7) Nacci, C.; Baroncini, M.; Credi, A.; Grill, L. Reversible Photoswitching and Isomer-Dependent Diffusion of Single Azobenzene Tetramers on a Metal Surface. *Angew. Chem., Int. Ed.* **2018**, *57*, 15034−15039.

(8) (a) Arramel; Pijper, T. C.; Kudernac, T.; Katsonis, N.; van der Maas, M.; Feringa, B. L.; van Wees, B. J. Reversible light induced conductance switching of asymmetric diarylethenes on gold: surface and electronic studies. *Nanoscale* **2013**, *5*, 9277−9282. (b) Irie, M. Diarylethenes for memories and switches. *Chem. Rev.* **2000**, *100*, 1685−1716.

(9) Klajn, R. Spiropyran-based dynamic materials. *Chem. Soc. Rev.* **2014**, *43*, 148−184.

(10) (a) Aprahamian, I. Hydrazone switches and things in between. *Chem. Commun.* **2017**, *53*, 6674−6684. (b) van Dijken, D. J.; Kovaříček, P.; Ihrig, S. P.; Hecht, S. Acylhydrazones as Widely Tunable Photoswitches. *J. Am. Chem. Soc.* **2015**, *137*, 14982−14991.

(11) (a) Irie, M.; Mohri, M. Thermally irreversible photochromic systems. Reversible photocyclization of diarylethene derivatives. *J. Org. Chem.* **1988**, *53*, 803−808. (b) Nakamura, S.; Irie, M. Thermally irreversible photochromic systems. A theoretical study. *J. Org. Chem.* **1988**, *53*, 6136−6138. (c) Irie, M. Diarylethenes for memories and switches. *Chem. Rev.* **2000**, *100*, 1685−1716. (d) Tian, H.; Yang, S. Recent progresses on diarylethene based photochromic switches. *Chem. Soc. Rev.* **2004**, *33*, 85−97. (e) Zhang, J. J.; Zou, Q.; Tian, H. Photochromic materials: more than meets the eye. *Adv. Mater.* **2013**, *25*, 378−399.

(12) (a) Pace, G.; Ferri, V.; Grave, C.; Elbing, M.; von Hänisch, C.; Zharnikov, M.; Mayor, M.; Rampi, M. A.; Samori, P. Cooperative light-induced molecular movements of highly ordered azobenzene self-assembled monolayers. *Proc. Natl. Acad. Sci. U. S. A.* **2007**, *104*, 9937−9942. (b) Schweighauser, L.; Strauss, M. A.; Bellotto, S.; Wegner, H. A. Attraction or repulsion? London dispersion forces control azobenzene switches. *Angew. Chem., Int. Ed.* **2015**, *54*, 13436−13439. Schweighauser, L.; Strauss, M. A.; Bellotto, S.; Wegner, H. A.

Anziehung oder Abstoßung? London-Dispersionswechselwirkungen kontrollieren Azobenzol-basierte molekulare Schalter. *Angew. Chem.* **2015**, *127*, 13636−13639. (c) Li, Q.; Qian, H.; Shao, B.; Hughes, R. P.; Aprahamian, I. Building strain with large macrocycles and using it to tune the thermal half-lives of hydrazone photochromes. *J. Am. Chem. Soc.* **2018**, *140*, 11829−11835.

(13) Schlimm, A.; Löw, R.; Rusch, T.; Röhricht, F.; Strunskus, T.; Tellkamp, T.; Sönnichsen, F.; Manthe, U.; Magnussen, O.; Tuczek, F.; Herges, R. Long-Distance Rate Acceleration by Bulk Gold. *Angew. Chem., Int. Ed.* **2019**, *58*, 6574−6578.

(14) Katsonis, N.; Kudernac, T.; Walko, M.; van der Molen, S. J.; van Wees, B. J.; Feringa, B. L. Reversible conductance switching of single diarylethenes on a gold surface. *Adv. Mater.* **2006**, *18*, 1397−1400.

(15) Kumar, A. S.; Ye, T.; Takami, T.; Yu, B.-C.; Flatt, A. K.; Tour, J. M.; Weiss, P. S. Reversible photo-switching of single azobenzene molecules in controlled nanoscale environments. *Nano Lett.* **2008**, *8*, 1644−1648.

(16) Durr, H. Perspectives in Photochromism: A Novel System Based on the 1, 5-Electrocyclization of Heteroanalogous Pentadienyl Anions. *Angew. Chem., Int. Ed. Engl.* **1989**, *28*, 413−431.

(17) (a) Bandara, H. M. D.; Burdette, S. C. Photoisomerization in different classes of azobenzene. *Chem. Soc. Rev.* **2012**, *41*, 1809−1825. (b) Landge, S. M.; Tkatchouk, E.; Benitez, D.; Lanfranchi, D. A.; Elhabiri, M.; Goddard, W. A.; Aprahamian, I. Isomerization mechanism in hydrazone-based rotary switches: lateral shift, rotation, or tautomerization? *J. Am. Chem. Soc.* **2011**, *133*, 9812−9823.

(18) (a) Napper, A. M.; Liu, H.; Waldeck, D. H. The Nature of Electronic Coupling between Ferrocene and Gold through Alkanethiolate Monolayers on Electrodes: The Importance of Chain Composition, Interchain Coupling, and Quantum Interference. *J. Phys. Chem. B* **2001**, *105*, 7699−7707. (b) Comstock, M. J.; Levy, N.; Kirakosian, A.; Cho, J.; Lauterwasser, F.; Harvey, J. H.; Strubbe, D. A.; Frechet, J. M. J.; Trauner, D.; Louie, S. G.; Crommie, M. F. Reversible photomechanical switching of individual engineered molecules at a metallic surface. *Phys. Rev. Lett.* **2007**, *99*, 38301.

(19) (a) Zhou, X.-L.; Zhu, X.-Y.; White, J. M. Photochemistry at adsorbate/metal interfaces. *Surf. Sci. Rep.* **1991**, *13*, 73−220. (b) Wen, J.; Li, W.; Chen, S.; Ma, J. Simulations of molecular self-assembled monolayers on surfaces: packing structures, formation processes and functions tuned by intermolecular and interfacial interactions. *Phys. Chem. Chem. Phys.* **2016**, *18*, 22757−22771. (c) Pourghaz, Y.; Dongare, P.; Thompson, D. W.; Zhao, Y. Click functionalized poly(p-phenylene ethynylene)s as highly selective and sensitive fluorescence turn-on chemosensors for Zn^{2+} and Cd^{2+} ions. *Chem. Commun.* **2011**, *47*, 11014−11016.

(20) Alemani, M.; Selvanathan, S.; Ample, F.; Peters, M. V.; Rieder, K. H.; Moresco, F.; Joachim, C.; Hecht, S.; Grill, L. Adsorption and switching properties of azobenzene derivatives on different noble metal surfaces: Au (111), Cu (111), and Au (100). *J. Phys. Chem. C* **2008**, *112*, 10509−10514.

(21) Sprague-Klein, E. A.; Negru, B.; Madison, L. R.; Coste, S. C.; Rugg, B. K.; Felts, A. M.; McAnally, M. O.; Banik, M.; Apkarian, V. A.; Wasielewski, M. R.; Ratner, M. A.; Seideman, T.; Schatz, G. C.; Van Duyne, R. P. Photoinduced Plasmon-Driven Chemistry in trans-1,2-Bis(4-pyridyl)ethylene Gold Nanosphere Oligomers. *J. Am. Chem. Soc.* **2018**, *140*, 10583−10592.

(22) (a) Wang, X.; Huang, S.-C.; Huang, T.-X.; Su, H.-S.; Zhong, J.-H.; Zeng, Z.-C.; Li, M.-H.; Ren, B. Tip-enhanced Raman spectroscopy for surfaces and interfaces. *Chem. Soc. Rev.* **2017**, *46*, 4020−4041. (b) Anderson, M. S. Locally enhanced Raman spectroscopy with an atomic force microscope. *Appl. Phys. Lett.* **2000**, *76*, 3130−3132. (c) Hayazawa, N.; Inouye, Y.; Sekkat, Z.; Kawata, S. Metallized tip amplification of near-field Raman scattering. *Opt. Commun.* **2000**, *183*, 333−336. (d) Pettinger, B.; Schambach, P.; Villagómez, C. J.; Scott, N. Tip-enhanced Raman spectroscopy: near-fields acting on a few molecules. *Annu. Rev. Phys. Chem.* **2012**, *63*, 379−399. (e) Wickramasinghe, H. K.; Chaigneau, M.; Yasukuni, R.; Picardi, G.; Ossikovski, R. Billion-fold increase in tip-enhanced Raman signal. *ACS Nano* **2014**, *8*, 3421−3426. (f) Zhang, R.; Zhang, Y.; Dong, Z. C.; Jiang, S.; Zhang, C.; Chen, L. G.; Zhang, L.; Liao, Y.; Aizpurua, J.; Luo, Y.; Yang, J. L.; Hou, J. G. Chemical mapping of a single molecule by plasmon-enhanced Raman scattering. *Nature* **2013**, *498*, 82−86. (g) Zhong, J.-H.; Jin, X.; Meng, L.; Wang, X.; Su, H.-S.; Yang, Z.-L.; Williams, C. T.; Ren, B. Probing the electronic and catalytic properties of a bimetallic surface with 3 nm resolution. *Nat. Nanotechnol.* **2017**, *12*, 132−136.

(23) Tallarida, N.; Rios, L.; Apkarian, V. A.; Lee, J. Isomerization of one molecule observed through tip-enhanced Raman spectroscopy. *Nano Lett.* **2015**, *15*, 6386−6394.

(24) Zheng, L.-Q.; Wang, X.; Shao, F.; Hegner, M.; Zenobi, R. Nanoscale Chemical Imaging of Reversible Photoisomerization of an Azobenzene-Thiol Self-Assembled Monolayer by Tip-Enhanced Raman Spectroscopy. *Angew. Chem., Int. Ed.* **2018**, *57*, 1025−1029.

(25) (a) Love, J. C.; Estroff, L. A.; Kriebel, J. K.; Nuzzo, R. G.; Whitesides, G. M. Self-Assembled Monolayers of Thiolates on Metals as a Form of Nanotechnology. *Chem. Rev.* **2005**, *105*, 1103−1169. (b) Claridge, S. A.; Liao, W.-S.; Thomas, J. C.; Zhao, Y.; Cao, H. H.; Cheunkar, S.; Serino, A. C.; Andrews, A. M.; Weiss, P. S. From the bottom up: dimensional control and characterization in molecular monolayers. *Chem. Soc. Rev.* **2013**, *42*, 2725−2745.

(26) Zheng, Y. B.; Payton, J. L.; Weiss, P. S.; et al. Surface-enhanced Raman spectroscopy to probe reversibly photoswitchable azobenzene in controlled nanoscale environments. *Nano Lett.* **2011**, *11*, 3447−3452.

(27) Merrick, J. P.; Moran, D.; Radom, L. An evaluation of harmonic vibrational frequency scale factors. *J. Phys. Chem. A* **2007**, *111*, 11683−11700.

(28) Shao, B.; Baroncini, M.; Qian, H.; Bussotti, L.; Di Donato, M.; Credi, A.; Aprahamian, I. Solution and Solid-State Emission Toggling of a Photochromic Hydrazone. *J. Am. Chem. Soc.* **2018**, *140*, 12323−12327.

(29) Wolf, M.; Tegeder, P. Reversible molecular switching at a metal surface: A case study of tetra-*tert*-butyl-azobenzene on Au (111). *Surf. Sci.* **2009**, *603*, 1506−1517.

(30) (a) Wuelfing, W. P.; Green, S. J.; Pietron, J. J.; Cliffel, D. E.; Murray, R. W. Electronic Conductivity of Solid-State, Mixed-Valent, Monolayer-Protected Au Clusters. *J. Am. Chem. Soc.* **2000**, *122*, 11465−11472. (b) Wang, G. R.; Wang, L.; Rendeng, Q.; Wang, J.; Luo, J.; Zhong, C.-J. Correlation between nanostructural parameters and conductivity properties for molecularly-mediated thin film assemblies of gold nanoparticles. *J. Mater. Chem.* **2007**, *17*, 457−462. (c) Avila, A.; Gregory, B. W.; Niki, K.; Cotton, T. M. An Electrochemical Approach to Investigate Gated Electron Transfer Using a Physiological Model System: Cytochrome c Immobilized on Carboxylic Acid-Terminated Alkanethiol Self-Assembled Monolayers on Gold Electrodes. *J. Phys. Chem. B* **2000**, *104*, 2759−2766.

(31) (a) Guo, L.-H.; Facci, J. S.; Mclendon, G. Distance dependence of electron transfer rates in bilayers of a ferrocene Langmuir-Blodgett monolayer and a self-assembled monolayer on gold. *J. Phys. Chem.* **1995**, *99*, 8458−8461. (b) Khoshtariya, D. E.; Dolidze, T. D.; Sarauli, D.; van Eldik, R. High-Pressure Probing of a Changeover in the Charge-Transfer Mechanism for Intact Cytochrome c at Gold/Self-Assembled Monolayer Junctions. *Angew. Chem., Int. Ed.* **2006**, *45*, 277−281. (c) Closs, G. L.; Miller, J. R. Intramolecular long-distance electron transfers in organic molecules. *Science* **1988**, *240*, 440−447.

(32) Kim, Y.; Wilson, A. J.; Jain, P. K. The Nature of Plasmonically Assisted Hot-Electron Transfer in a Donor−Bridge−Acceptor Complex. *ACS Catal.* **2017**, *7*, 4360−4365.

DOI: 10.1021/jacs.9b07057
J. Am. Chem. Soc. 2019, 141, 17637−17645